Accepted Manuscript

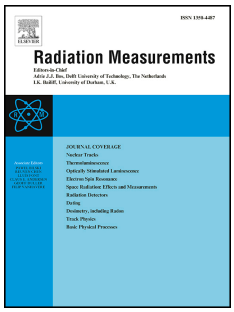

Thermoluminescence of $SrAl_2O_4:Eu^{2+}$, Dy^{3+}: Kinetic analysis of a composite-peak

M.L. Chithambo, A.H. Wako, A.A. Finch

PII: S1350-4487(16)30454-1

DOI: 10.1016/j.radmeas.2016.12.009

Reference: RM 5678

To appear in: *Radiation Measurements*

Received Date: 26 May 2016

Revised Date: 19 December 2016

Accepted Date: 20 December 2016

Please cite this article as: Chithambo, M.L., Wako, A.H., Finch, A.A., Thermoluminescence of $SrAl_2O_4:Eu^{2+}$, Dy^{3+}: Kinetic analysis of a composite-peak, *Radiation Measurements* (2017), doi: 10.1016/j.radmeas.2016.12.009.

Thermoluminescence of $SrAl_2O_4:Eu^{2+}$, Dy^{3+}: Kinetic analysis of a composite-peak

M. L. Chithambo[1*], A.H. Wako[2], A.A. Finch[3]

[1]*Department of Physics and Electronics, Rhodes University, PO BOX 94, Grahamstown 6140, South Africa*
[2]*Department of Physics, Meru University of Science and Technology, PO BOX 972-60200, Meru, Kenya*
[3]*Department of Physics and Electronics, University of St Andrews, Scotland*

Abstract

The kinetic analysis of thermoluminescence of beta-irradiated $SrAl_2O_4:Eu^{2+},Dy^{3+}$ is reported. The glow-curve is dominated by an apparently-single peak. It has been demonstrated using a number of tests including partial dynamic-heating, isothermal heating, phosphorescence and, the effect of fading, that the peak and the glow-curve consists of a set of closely-spaced peaks. In view of the peak being complex, its first few components were abstracted and analysed and for comparison, the peak was also analysed assuming it is genuinely single. In the latter, the order of kinetics is calculated to be intermediate between first and second-order and not first-order as predicted by qualitative tests such as the $T_m - T_{stop}$ or $T_m - dose$ procedures. A model based on density of energy states has been used to account for and reconcile the qualitative and quantitative results. The activation energy is found as ~1 eV, consistent with the value expected of Dy^{2+}, the presumed electron trapping state of the Dy^{3+} electron trap. The thermoluminescence is subject to thermal quenching with an activation energy of 0.520 ± 0.002 eV. The luminescence is ascribed to 5d→4f[7] Eu^{2+} transitions whereas the thermal quenching is presumed to occur from an alternative level of the degenerate 5d energy level of the Eu^{2+} cation.

Keywords: Thermoluminescence; kinetic-analysis; $SrAl_2O_4:Eu^{2+},Dy^{3+}$; thermal quenching; collocation

PACS: 78.60.Kn

*Corresponding author: Tel.:+27 46 6038450; fax:+27 46 603 8757
Email address: M.Chithambo@ru.ac.za (M. L. Chithambo)

1. Introduction

If the apparently simple thermoluminescence glow-peak in $SrAl_2O_4:Eu^{2+},Dy^{3+}$ is anything but, how should it be analysed for kinetic parameters?

The question of how to deal with glow-peaks that are not adjacent but embedded within one another is not posed often enough and is the subject of this report on $SrAl_2O_4:Eu^{2+},Dy^{3+}$, a well-known phosphor (Matsuzawa et al., 1996). Evidence for such collocation has been reported by Chithambo and Niyonzima (2014) in $Sr_2SiO_4:Eu^{2+}$ and by Mokoena et al. (2015) for $Ca_5(PO_4)_3OH:Gd^{3+},Pr^{3+}$. Evidence in terms of quasi-continuum distribution of activation energies has been described by, for example, Bos et al. (2011) for a number of phosphors including $SrAl_2O_4:Eu^{2+},Dy^{3+}$. Despite this, the number of reports where thermoluminescence from $SrAl_2O_4:Eu^{2+},Dy^{3+}$ is discussed with indifference to the complexity introduced by presence of closely-overlapping peaks is concerning.

The conventional description of thermoluminescence assumes the presence of localised and discrete energy levels within the band gap. Since the study of thermoluminescence is aided by kinetic analysis, analysis of glow-peaks for kinetic parameters is a common practical concern. However, if a method applicable to an isolated peak is used to analyse one that is not, the results may be invalid. Since most kinetic analysis methods only apply for isolated peaks, it is necessary to develop procedures for addressing collocation, that is, cases where multiple subsidiary peaks are concealed within a dominant one to such an extent that the collection appears as one. The glow-curve of $SrAl_2O_4:Eu^{2+}, Dy^{3+}$ e.g. (Matsuzawa et al., 1996) consists of a glow-peak with a wide expanse of the order of 100^{o}. Previous kinetic analyses of the peak e.g. (Kshatri et al., 2013) imply a tacit assumption that it is simple and single. However, some experimental studies of phosphors with similar features, namely $Ca_5(PO_4)_3OH:Gd^{3+},Pr^{3+}$ (Mokoena et al., 2015) or $Sr_2SiO_4:Eu^{2+}$ (Chithambo and Niyonzima, 2014) show evidence of peak-collocation. Therefore simply associating a prominent peak with a single discrete electron trap potentially disregards other peaks concealed within the peak-profile and leads to incomplete conclusions about the mechanisms in the thermoluminescence.

The number of methods to separate non-adjacent concealed peaks is limited. One technique uses ultraviolet light of various wavelengths to ionise electron traps and thereby generate a

range of activation energy values (Bos et al., 2011). This is accepted as indirect evidence of closely-spaced electron traps. Chithambo and Niyonzima (2014) and Mokoena et al. (2015) used a combination of isothermal and dynamic heating to digitally muster components of collocated peaks in $Ca_5(PO_4)_3OH:Gd^{3+},Pr^{3+}$ and $Sr_2SiO_4:Eu^{2+}$ and hence demonstrate the existence of closely-spaced peaks. To our knowledge, there are no other methods for experimentally separating collocated peaks.

This paper is concerned with the kinetic analysis of the prominent peak in $SrAl_2O_4:Eu^{2+},Dy^{3+}$. We report methods for separating closely-spaced peaks as a means to analyse a composite peak. For instructive reasons, we also show results obtainable when the same peak is analysed as though it were genuinely single. The report includes a study of thermal quenching, considers the analysis and interpretation of phosphorescence, describes fading and discusses models of mechanisms in the thermoluminescence.

2. Experimental methods

$SrAl_2O_4:Eu^{2+},Dy^{3+}$ used was prepared using combustion of an appropriately prepared solution. Measurements of the excitation and emission features; energy dispersive X-ray spectrometry to confirm the elements composition of the sample, X-ray diffraction to determine its crystal structure and scanning electron microscopy to show its morphology have been described in detail by Wako (2015). These are not essential for discussion of thermoluminescence and have been summarized in an accompanying online supplement.

Thermoluminescence was measured using a RISØ TL/OSL DA-20 Luminescence Reader. The luminescence was detected by an EMI 9235QB photomultiplier tube through a combination of a BG-39 bandpass filter (transmission band ~335 – 610 nm FWHM) and a BG-3 bandpass filter (transmission band ~250 – 600 nm FWHM). Samples, placed on stainless steel discs of diameter 10 mm and thickness 0.3 mm, were irradiated to required dose using a $^{90}Sr/^{90}Y$ beta source at 0.10 Gy s^{-1}. Measurements were made in a nitrogen atmosphere to avoid spurious signals from air.

Thermoluminescence was augmented by X-ray excited optical luminescence (XEOL) otherwise known as radioluminescence (RL) which is the luminescence emitted during X-ray irradiation. With the luminescence recorded as a function of the emission wavelength, this

method facilitates studies on how the emission band is affected by factors like irradiation dose (King et al., 2011). Our aim was to identify emission bands of stimulated luminescence in $SrAl_2O_4:Eu^{2+}$, Dy^{3+}. The synonymous use of XEOL and RL e.g. (Chithambo et al., 2015; King et al., 2011) should not be confused with XEOL where the luminescence is measured as a function of the X-ray energy.

XEOL measurements were carried out in ~1 mbar vacuum by heating to 400°C at 10 K min^{-} using the system reported by Luff and Townsend (1993). Samples were irradiated using a Philips MCN-101 X-ray tube at a dose rate of 1.8 Gy min^{-1}.

3. X-ray excited optical luminescence spectra

Figure 1 shows XEOL spectra of $SrAl_2O_4:Eu^{2}$, Dy^{3+}. Figure 1(a) is an isometric plot whereas Fig. 1(b) is the corresponding contour map. There are two prominent emissions, one at 475 nm and a more intense one at 575 nm. In particular, with reference to the intensity scale, there is evidence of increasing non-radiative transitions up to ~75^{o}C in the emission at 475 nm and up to 125^{o}C in the emission at 575 nm. There are also weaker emissions at about 405, 510, 600, 610 and 660 nm. It should be noted that Fig. 1 shows stimulated luminescence which should be distinguished from spontaneously emitted luminescence such as fluorescence. Various wavelengths in the emission spectrum of $SrAl_2O_4;Eu^{2+},Dy^{3+}$ were also measured by way of phosphorescence using a Cary Eclipse luminescence spectrometer (model LS-55) following excitation at 293 nm. Emission peaks were observed at 480, 490, 572, 615 and 665 nm. These are near those at 475, 575, 600, 610 and 660 nm in the XEOL spectra.

The peaks at 480 and 490 nm are attributed to $4f^{6}5d^{1}\leftrightarrow 4f^{7}$ transition of Eu^{2+} which substitutes for Sr^{2+} (Nakamura et al., 2000). The emissions at 572, 615 and 665 nm respectively correspond to $^{5}D_{0}\rightarrow{}^{7}F_{1}$, $^{5}D_{0}\rightarrow{}^{7}F_{2}$ and $^{5}D_{0}\rightarrow{}^{7}F_{3}$ transitions of Eu^{3+} ions (Cannas et al., 2006).

4. General features of the thermoluminescence glow-curve

4.1 Glow-curve features

Figure 2 shows a glow-curve measured at 1^{o}C s^{-1} after irradiation to 20 Gy. The glow-curve is dominated by a peak at 34^{o}C. Whether this is a simple peak will be examined in the text.

The peak is preceded by phosphorescence before the onset of thermoluminescence. The increase in signal beyond 400^{o}C is due to blackbody radiation. The inset shows natural thermoluminescence measured at 1^{o}C s^{-1}. This is the luminescence owing to natural radiation since any event that erased residual charge from electron traps. For the sample, the event is heating to 500^{o}C during synthesis. The glow-curve shows three peaks at 74, 170 and 340^{o}C. The existence of such natural thermoluminescence prior to any laboratory irradiation is evidence of notable sensitivity of the material to natural irradiation. It should be noted that the peak at 34^{o}C is absent in the natural thermoluminescence.

4.2 Order of kinetics

In order to determine the order of kinetics of the apparently single peak, the $T_m - T_{stop}$ procedure was used. Three sets of measurement corresponding to 20, 60 and 100 Gy were made. An irradiated sample was partially heated from 20 to 22^{o}C and after cooling to 20^{o}C, heated again to 500^{o}C to obtain the complete glow-curve. The position T_m of the resultant peak was noted. The procedure was repeated with T_{stop} increased in turn by 2^{o}C up to 60^{o}C. For each dose, five measurements were used to obtain an average of T_m with its uncertainty ΔT_m being the standard deviation of the set.

Figure 3(a) shows the peak temperature T_m against T_{stop} for the three sets of measurement. The position T_m increases non-monotonically with T_{stop}. Between 20 and 50^{o}C, T_m changes slowly with T_{stop} and, for each dose, there are regions where T_m is independent of T_{stop}. An example is the portion from 20 through 26^{o}C for measurements corresponding to 60 Gy (solid triangles). The detailed dependence of T_m on T_{stop} between 20 and 30^{o}C is illustrated in Fig. 3(b) for measurements at 1^{o}C intervals on another sample. The latter further shows that in increasing with T_{stop}, T_m initially goes through regions in which it is independent of T_{stop}. According to TL theory (Pagonis et al, 2006), each such flat region corresponds to a TL peak. In further examination of the dependence of T_m on T_{stop} between 42 and 60^{o}C (Fig. 3a, inset) by linear regression, it was found that the slopes corresponding to 20, 60 and 100 Gy were 1.16 ± 0.04, 0.93 ± 0.05 and 1.02 ± 0.05. The increase of T_m with T_{stop} suggests that the apparently single peak is a composite. In particular, a straight line of slope close to 1, as found, is expected for a quasi-continuum set of first or second-order peaks (Pagonis et al, 2006). Since this result is characteristic of first or second-order kinetics, it is not possible on

this evidence alone to deduce the order of kinetics for the peak. Further tests to address this question are necessary and will be described.

4.3 Influence of irradiation on peak position

The dependence of T_m on dose is characteristic of the order of kinetics and complements the $T_m - T_{stop}$ method. The position of a first-order peak is independent of dose whereas that of a second-order decreases with dose (Chen and Mckeever, 1997).

Figure 4 shows T_m against dose. The peak temperature increases with dose up to 155 Gy but through regions in which it is independent of dose. Ostensibly therefore, the apparently single peak of Fig. 2 consists of multiple first-order peaks which individually become prominent at specific irradiation doses.

The increase of peak position with dose, which was also observed for ɤ-irradiated $SrAl_2O_4:Eu^{2+},Dy^{3+}$ (Bedyal et al., 2013), is anomalous and cannot be accounted for by either first or second-order kinetics. Such behaviour has also been reported before in $Ca_5(PO_4)_3OH:Gd^{3+},Pr^{3+}$ (Mokoena et al., 2015). Figure 4 can be explained along the same lines used to discuss a similar feature in quartz and in $Ca_5(PO_4)_3OH:Gd^{3+},Pr^{3+}$. The increase of T_m with T_{stop} (Fig. 3) is consistent with the main peak being a composite. Since a first-order peak is independent of dose, the existence of regions where T_m is not affected by dose suggests that the main peak consists of multiple first-order peaks each of which becomes dominant depending on the dose used. This produces a plot where T_m appears to increase with dose. For some doses, the glow-curve is dominated by a particular component and T_m then appears to be independent of dose until the onset of another higher dose range. The qualitative interpretations of Figs. 3 and 4 thus far are based on standard theories of thermoluminescence. We will experimentally examine the premise that the apparently single peak of Fig. 2 consists of several overlapping components.

4.4 Dose response

Figure 5 shows the dose response for the apparently-single peak for doses between 10 and 155 Gy i.e. the same range as for Fig. 4. The intensities correspond to peak heights. The growth-curve was examined using the superlinearity index $g(D)$ given by

$$g(D) = \left[\frac{\mathrm{Dy"(D)}}{\mathrm{y'(D)}}\right] + 1, \qquad (1)$$

where $y(D)$ is the analytical dose dependence of the intensity, $y'(D)$ and $y''(D)$ are respectively the first and second derivative of $y(D)$ (Pagonis et al, 2006). The dose response is linear with a superlinearity index equal to 1. The inset shows examples of glow-curves corresponding to 20, 60, 123 and 155 Gy. As evident, when dose is increased, the intensity of the peak increases, it shifts to higher temperatures and no new peaks appear. Since the peak consists of multiple components, the intensity at each dose should be that of the dominant component.

The possibility of the peak fading during irradiation was considered. If there were significant loss of signal during irradiation, the shape of the glow-peak in question would be affected and the change would be pronounced for short irradiations and short delays between irradiation and measurement. The same feature would show up for thermoluminescence measured after irradiation to a similar dose by two different sources of unequal dose rates.

Figure 6(a) shows the main peak measured at 1^{o}C s^{-1} after nominal delays of 0, 5 and 10 s between irradiation to 1 Gy and measurement respectively. The shape of the peak is not influenced by the delay meaning that fading if at all present, is negligible. Figure 6(b) shows a glow-curve measured after beta-irradiation to ~18.9 Gy at 0.10 G s^{-1}. This is to be compared with Fig. 6(c) measured after X-ray irradiation to 18 Gy at 0.03 Gy s^{-1}. The latter is subject to phosphorescence in its rising edge. Figures 6(b) and (c) show that the change of either irradiation source or dose rate does not affect the shape of the peak confirming that the peak does not fade during irradiation.

5. Glow-curve resolution

The dependence of T_m on T_{stop} and on dose imply that the simple peak of Fig. 2 consists of collocated components. We assume that the features measured at a particular dose represent the most dominant component. We examine this idea experimentally using three methods namely, partial heating akin to the fractional glow technique, isothermal heating and, obliquely by observing the influence of fading on the peak.

5.1 Glow-curve resolution by partial heating

The aim of this study was to investigate the presence of any components of the main peak as well as throughout the glow-curve. A sample irradiated to 20 Gy was partially heated to 40^{o}C at 1.0^{o}C/s to remove the peak at 34^{o}C s^{-1}. The sample was then cooled to room temperature after which it was heated again to 400^{o}C in order to monitor the position of the first remnant peak. The experiments were repeated with the preheating temperature incremented by 5^{o}C each time up to 270^{o}C. This exercise was intended to search for collocated peaks and not necessarily to find *all* such peaks.

Figure 7(a) shows glow-peaks obtained after partial heating as described. As each resultant peak is removed by partial heating, previously concealed ones successively appear. Thus for example, the peak measured after preheating to 40℃ (open circles) and 60℃ (open squares) are different. Each new peak after partial heating is itself made up of collocated components.

Figure 7(b) shows all peaks corresponding to 5℃ intervals in the partial heating. This result shows that what appears as a single peak is indeed a collection of closely spaced ones. This is evident in Fig. 7(b) up to 240℃ beyond which the existence of any peaks is not obvious. However, as the inset shows, the same procedure reveals distinct peaks at 190℃ and 330℃ after preheating to 180 and 270℃. Fig. 7 experimentally verifies that both the main peak and the glow-curve as a whole consist of closely-spaced peaks.

5.2 Glow-curve deconvolution using isothermal heating

Where one peak is embedded within another, they cannot be separated using thermal cleaning which relies on heating beyond an identified peak-maximum to reveal the adjacent peak. Therefore, the glow-curve was also resolved into its components using isothermal heating.

The basis of the method e.g (Chithambo and Niyonzima, 2014) is that if a sample is held for a time at a temperature corresponding to a position on the rising edge of a peak, the isothermal heating depletes the first peak in the series to reveal the next one it is collocated with.

Figure 8 exemplifies some components of the glow-curve recovered using isothermal-heating at 80, 130, 240, 330 and 380℃ for 100 s respectively after irradiation to 100 Gy in each case. This is further evidence that the glow-curve is a conglomeration of closely-spaced peaks.

5.3 Fading as a means for glow-curve resolution

The influence of delay between irradiation and measurement on the thermoluminescence intensity was studied on one aliquot for delays up to 21600 s. The experiments offered an incidental means to address the possibility that the main peak consists of multiple closely-spaced components.

Figure 9(a) shows the influence of delayed stimulation on the main peak. The abscissa is truncated at 120℃ to better show the result. The luminescence intensity fades with time and the apparent peak-position increases (inset). The fading cannot be explained by thermally-induced loss of charge from one electron trap because if this were the case, the intensity would decrease but the peak-position would either be unaffected or increase. Figure 9(a) shows that the peak shifts by as much as 40℃, improbable for a single peak. We interpret the change as due to loss of signal from multiple electron traps decaying at different rates. The fading of a less stable peak at a lower temperature enables a subsequent one at a higher temperature in the series to appear. Figure 9(a) is further evidence that the glow-curve consists of multiple closely-spaced peaks.

The peak fades due to loss of signal as phosphorescence. Phosphorescence is the emission of thermoluminescence as a function of time at a constant temperature and its time-dependence for first-order kinetics at temperature T is exponential, that is,

$$I(t) = I_o exp(-pt), \qquad (2)$$

where I_o is the initial intensity and p is the probability of thermal stimulation. The corresponding expression for general-order kinetics is

$$I(t) = \frac{n_o^b p''}{[1 + (b-1)p'' n_o^{b-1} t]^{b/(b-1)}}, \qquad (3)$$

where b is the order of kinetics and p'' the decay constant in this case.

Figure 9(b) shows the phosphorescence measured from another aliquot for 30000 s after irradiation to 100 Gy. The phosphorescence could not be described by Eqs. (2) or (3), a sum of decaying exponential functions which apply for electron de-trapping from a single electron trap or even by forms of the experimental Becquerel decay law,

$$I(t) = \frac{I_o}{(1 + ct)} \qquad (4)$$

where *c* is a constant and I_o the initial value. We therefore modelled the rate of change of the phosphorescence intensity as

$$\frac{dI}{dt} = \frac{-\kappa I}{(t + \gamma)^2} \qquad (5)$$

from which

$$I(t) = A \exp\left(\frac{\kappa}{t+\gamma}\right) \qquad (6)$$

where A is a constant, $\gamma$is a scaling parameter whose presence ensures that the intensity is not rendered asymptotic with respect to *t* in order to be consistent with experimental results. The solid line through data points in Fig. 9(b) is the best fit of Eq. (6) which like the Becquerel law, is empirical. The important point here is that the phosphorescence that causes fading of the apparently-single peak cannot be modelled on the basis of a single electron trap.

Figure 9(c) shows how the glow-curve fades as phosphorescence is emitted by comparing a glow-curve measured immediately after irradiation (open circles) with one measured after 30000 s. To ease comparison, the intensity of the initial glow-curve has been scaled down by 96%. The main peak had faded completely by 30000 s after irradiation. In contrast, peaks near and beyond 100^{o}C were less affected. Thus the phosphorescence of Fig. 9(b) is due to loss of electrons from electron traps responsible for the main peak. Such a depletion of charge from multiple electron traps explains why the phosphorescence cannot be modelled as an exponential decay. To examine this premise further, phosphorescence was measured from a sample where the main peak had been removed by preheating to 100^{o}C after irradiation to 100 Gy. The inset to Fig. 9(c) shows the result where it is apparent that no phosphorescence was observed in the absence of the main peak. Figures 9(b) and (c) is incidental evidence that the main peak consists of serried components.

6. Kinetic analysis

We have demonstrated that the prominent thermoluminescence peak consists of closely-spaced components. Methods for separating and analysing non-adjacent peaks are not readily available. Conventional procedures for dealing with thermoluminescence peaks apply to either isolated peaks or overlapping ones with identifiable peak maxima. Apart from extracting and analysing the components separately, the question that needs to be addressed is whether such methods can reliably be used to analyse a composite peak and if so how this can be done and the result interpreted. In view of this, kinetic analysis was carried out in two ways, using methods that avoid or minimise the influence of one peak on another for example peak-position methods and, for comparison, methods that exploit the whole peak thereby assuming that the peak is genuinely simple and single.

6.1 Variable heating rate method

6.1.1 Calculation of kinetic parameters

The variable heating rate technique (see Chen and Mckeever, 1997) was applied on samples irradiated to 10, 20, 60 and 100 Gy for heating from 0.2 to 4°C s^{-1}. Five measurements were made for each dose. The activation energy E corresponding to 10 and 20 Gy was calculated as 1.07 ± 0.06 eV whereas for 60 and 100 Gy this was 1.18 ± 0.02 eV and 1.17 ± 0.03 eV respectively. The frequency factor s was evaluated as 4.1×10^{16} s^{-1} for the 10 and 20 Gy data and 1.8×10^{18} s^{-1} and 8.8×10^{17} s^{-1} corresponding to 60 and 100 Gy respectively. The values of s are anomalously high and are inconsistent with the interpretation that they are a measure of the frequency with which a bound electron attempts to detach from its binding potential which would be of the order of 10^{12} s^{-1}. The reason for this is not clear but Chen and Hag-Yahya (1996) explained this in LiF as an artefact caused by competition between electron traps and non-radiative centres.

6.1.2 Influence of heating rate on thermoluminescence intensity

Measurements to study the influence of heating rate on thermoluminescence intensity were made 5 times each on an aliquot irradiated to 10, 20, 60 and 100 Gy using heating rates from 0.2 to 4°C s^{-1}. Since the main peak is subject to phosphorescence on its rising edge, the intensities were monitored at the peak maximum rather than as the area under the glow-peak in order to prevent the effect of peak-collocation. Figure 10(a) which compares glow-curves

measured at 0.4°Cs $^{-1}$ (open circles) 0.8°Cs $^{-1}$ (open squares) and 3°Cs $^{-1}$ shows that the thermoluminescence intensity decreases with heating rate. The inset shows the same feature but as a plot of peak-intensity against heating rate. Such a change indicates that the peak in question, the main peak here, is affected by thermal quenching (Pagonis et al., 2006), that is, increasing incidences of non-radiative recombination as the position of the peak shifts to higher temperatures. It should be noted that the thermal quenching in Fig. 10(b) was quantified using intensity values instead of area because the peak is considered to be a composite and so cannot be associated with a unique area. When normalised against change in heating rate, areas are more consistent with heating rate than peak intensities. Therefore the use of intensity in Fig. 10(b), where use of area is invalid, should be regarded only as an estimate. We stress that the method of calculation of thermal quenching parameters using peak intensities has severe shortcomings and use of peak intensities is preferable where possible.

If the thermoluminescence corresponding to the lowest heating rate is associated with the least amount of quenching, then its intensity I_u is related to the subsequent quenched ones $I_q(T)$ measured at higher heating rates as

$$I_q(T) = \frac{I_u}{1+C\ exp\left(-\frac{\Delta E}{kT_m}\right)}, \qquad (7)$$

where ΔE is the activation energy of thermal quenching, $C = \nu\tau_{rad}$ where τ_{rad} is the radiative lifetime at absolute zero of temperature and ν is the frequency factor applicable to the non-radiative process. It needs to be stressed that I_u is constant and is only associated with the lowest heating rate in a set. The thermal quenching evident in Fig. 10(a) was quantified by plotting ln $[(I_u/I_q) - 1)]$ against $1/kT_m$ as shown in Fig. 10(b). The value of ΔE corresponding to 60 and 100 Gy was calculated as 0.54 ± 0.01 eV and 0.520 ± 0.002 eV respectively. For C, a typical value was 4.7 x 10^8. The mechanisms involved in the thermal quenching will be discussed later.

6.2 Curve-fitting

6.2.1 Curve-fitting of the main peak as a supposed single peak

For instructive reasons, we now analyse the peak as simple and single to demonstrate results obtainable under such an assumption.

The thermoluminescence was analysed on the basis of general-order kinetics using the model of Kitis (1998). Since thermal quenching had been determined for the apparently-single main peak, the thermoluminescence intensity $I(T)$ was fitted by the expression

$$I(T) = \left\{ I_m b^{\frac{b}{b-1}} exp\left(\frac{E}{kT}\frac{T-T_m}{T_m}\right) \left[(b-1)(1-\Delta)\frac{T^2}{T_m^2} exp\left(\frac{E}{kT}\frac{T-T_m}{T_m}\right) + Z_m\right]^{\frac{-b}{b-1}} \right\} \eta(T) + \sum_{i=1}^{i=3} f_i(T), \quad 8)$$

where $f(T)$ is the same term within the braces, I_m is the peak maximum, T_m the corresponding peak temperature, $\Delta = 2kT/E$, $\Delta_m = 2kT_mE$, and $Z_m = 1 + (b-1)\Delta_m$ and $n\,(T)$ is the luminescence efficiency given by

$$n(T) = \frac{1}{1 + C\,\exp(-\Delta E/kT)}. \qquad (9)$$

The correction for thermal quenching was necessary because the measured thermoluminescence intensity is less than that predicted by the Kitis equation. Eq. (8) was used to account for four apparent peaks in the glow-curve (inset). The corresponding frequency factor was evaluated on the basis of general-order kinetics as

$$s = \frac{\beta E}{kT_m^2\left(1 + \frac{2kT_m(b-1)}{E}\right)} exp\left(\frac{E}{kT_m}\right), \qquad (10)$$

where all parameters are as previously defined.

Figure 11(a) shows the best fit of Eq. (8) for a sample irradiated to 60 Gy for which $E = 0.89 \pm 0.01$ eV and $b = 1.51 \pm 0.17$. The frequency factor was evaluated as 3.0×10^{13} s^{-1}. The first two terms recovered by glow-curve deconvolution are included for illustration only.

To ascertain whether the activation energy has any systematic dependence on dose, the curve fitting was done on glow-curves corresponding to a wide range of doses. Figure 11(b) shows the activation energy against dose. Allowing for statistical scatter, the activation energy is of the order of 0.90 eV and $b \sim 1.5$. Thus if the peak is analysed using curve-fitting as if it is a simple single peak, the order of kinetics is found to be general-order and not first-order as predicted by the $T_m - T_{stop}$ and $T_m - dose$ procedures.

6.2.2 Curve-fitting of digitally mustered components

Components of the main peak recovered by digital mustering (Chithambo and Niyonzima 2014) were analysed using the Kitis general-order expression (Kitis, 1998). The aim of digital-mustering is to separate peaks and obtain their complete shape to enable kinetic analysis. A peak at a relatively lower temperature is found by digitally subtracting a glow-peak obtained after partial heating from the initial glow-peak. Measurements were made at $1^{o}C\ s^{-1}$ on a sample irradiated to 20 Gy. Up to 32 glow-curves were obtained after partial heating to final temperatures from 40 through $270^{o}C$. Kinetic analysis was carried out on peaks digitally mustered by subtracting successive peaks as described. Figure 12(a) shows the first five components fitted with the Kitis model. For completeness, the first 10 of the 32 peaks obtained after partial heating are shown in Fig. 12(b). The order of kinetics for the first two components were found as 1.58 ± 0.08 and 1.41 ± 0.09 and the activation energy as 0.96 ± 0.04 and 0.88 ± 0.04 respectively. Apart from consistency with those in the preceding section, these results also suggest that when the components of the peak are analysed as described, the order of kinetics is found as general.

6.2.3 Kinetic analysis using the temperature-dependence of the area underneath an isothermal decay-curve

The phosphorescence measured at temperatures coincident with those of the main peak was analysed using the the temperature-dependence of the area underneath an isothermal decay-curve as described by Chithambo (2014). In the method, a series of data points corresponding to the area Φ under an isothermal decay-curve measured at a specific temperature for a specific time are plotted against the measurement temperature. The procedure produces a pseudo-peak as a means for kinetic analysis. The basis of the method is that since phosphorescence is thermoluminescence measured at a constant temperature, each data point Φ resembles a data point at that particular temperature were such data obtained contiguously in a dynamic run at a specific heating rate. Because this method cannot isolate components of a composite peak, it serves to also illustrate results obtainable when the peak is analysed as a *bona fide* single peak.

Figure 13 shows the dependence of the area Φ corresponding to 5 s on measurement temperature between 28 and $60^{o}C$ for runs corresponding to 20 and 100 Gy. The measurements were made on the same aliquot. Each data point was obtained between irradiation and heating to $400^{o}C$, the latter done to remove residual charge in electron traps.

The solid line through data points in Fig. 13 is the best fit of the Kitis general-order equation from which $b = 2.07 \pm 0.22$ and $E = 0.87 \pm 0.09$ eV for phosphorescence corresponding to 20 Gy and $b = 2.01 \pm 0.39$ and $E = 0.84 \pm 0.10$ eV for the 100 Gy data. The activation energy values are consistent with those from curve-fitting in sections 6.2.1 and 6.2.2 but the order of kinetics is found to be second-order.

6.2.4 Peak-shape method

The main peak was also analysed using the peak-shape method (Chen and McKeever, 1997) which exploits the full, lower and upper half-widths at half-maximum (ω,τ and δ). The activation energy corresponding to 20 Gy was ~0.88 eV and the geometrical factor $\mu_g = 0.50 \pm 0.10$ signifying general-order kinetics. The set of kinetic parameters found using various methods is listed in Table 1.

7. Fading of the main peak

The study of fading of the main peak is complicated by the fact that the various components of the peak fade at different rates as is apparent from Fig. 9. For this reason, the fading was monitored with respect to the position of the component (of the apparently single-peak) whose position was unchanged as the delay between irradiation and measurement was increased. This was done to ensure that only the intensity of a particular peak was noted in order to avoid the influence of peak-collocation on the result. Tests corresponding to irradiation to 20 Gy and heating at 1.0 ^{o}C/s showed that the position of the first component of the main peak remained within 42.0 ± 1.4^{o}C for delays up to 25 s. The fading was therefore only studied in this range because beyond 25 s, the peak position changed noticeably.

Figure 14 shows the intensity against delay between irradiation and measurement at room temperature. The intensity fades with delay but not exponentially as might be expected in thermal fading of a peak associated with a single electron trap. The fading observed in Fig. 14 cannot be explained by thermally-induced loss of charge from one electron trap alone because in this case the probability of charge release would produce a simple exponential decay (McKeever et al., 1995) which is not the case in Fig. 14. The time-dependent change of luminescence intensity could be quantified by an expression of the form of Eq. (6).

The form of the time-dependent decrease in intensity with delay was not influenced by whether the intensities were monitored as peak intensities or as areas under a peak up to ~100^{o}C, that is, measuring the first peak only. The solid line through the data points is the best fit of Eq. (6) attesting to the agreement between model and experimental data. It is not immediately clear what the cause of the fading behaviour in Fig. 14 is but loss of signal from more than one electron trap at different decay rates or even defect reactions during the delay between irradiation and measurement are possibilities that require further examination. The analysis shown in Fig. 14 is necessarily only approximate and the most accurate method would be to extract and monitor the change of particular components with delay between irradiation and measurement.

8. Mechanisms of thermoluminescence in $SrAl_2O_4:Eu^{2+},Dy^{3+}$

8.1 Explanation based on a discrete energy band scheme

There are four features relevant to explain the mechanisms of thermoluminescence in $SrAl_2O_4:Eu^{2+},Dy^{3+}$ as studied, namely, that $SrAl_2O4:Eu^{2+},Dy^{3+}$ shows natural thermoluminescence; its glow-curve has collocated peaks; it produces phototransferred thermoluminescence (Chernov et al; 2008) and that its thermoluminescence fades.

The existence of natural thermoluminescence, with peaks at 74, 170 and 340^{o}C (Fig. 2; inset), points to presence of some stable electron traps able to retain charge over considerable periods. The presence of closely-spaced peaks implies closely-spaced electron traps comprising shallow, intermediate-energy and deep traps. That deep traps are involved is also implicit in both the natural and phototransferred thermoluminescence. The fading of signal between irradiation and measurement during which phosphorescence is observed is evidence of shallow unstable electron traps. Phosphorescence also proceeds for periods much longer than required for the main peak to fade completely. We therefore speculate that there is thus a possibility that electrons transit from electron traps to the luminescence centre by quantum tunnelling.

It is evident that there are different types of electron traps involved in the TL of $SrAl_2O4:Eu^{2+},Dy^{3+}$. In this report we are concerned only with the apparently-single main peak. The electron trap for this peak is unknown and has never been verified. However, experimental evidence suggest that Dy^{3+} acts as an electron trap. For example, Swart et al., (2009) observed that the photoluminescence intensity from $SrAl_2O4:Eu^{2+},Dy^{3+}$ was less than that from $SrAl_2O4:Eu^{2+},Dy^{3+}$and put this down to Dy^{3+} acting as an electron trap. Wang et al., (2016), using both thermoluminescence and radioluminescence, observed Dy^{3+} emission lines in $SrAl_2O4:Eu^{2+},Dy^{3+}$ under radioluminescence but not during TL although $5d\rightarrow4f^7$ Eu^{2+} emission was apparent in both cases.

Although the mechanisms involved in the TL have not been unequivocally identified, one can speculate as to the processes involved. Dorenbos (2005a) proposed Dy^{3+} as an electron trap. After trapping an electron, Dy^{3+} is converted to Dy^{2+} electron-trapping state at 0.9 eV below the conduction band. In this sense, the defect that *will trap* an electron is defined as the

electron trap as opposed to one that has trapped an electron. The Eu^{2+} cation is the luminescence centre (Dorenbos et al., 2005a).

The $4f^7$ ground state of the Eu^{2+} luminescence centre and the 5d Eu^{2+} level are 3.2 eV and 0.017 eV below the conduction band respectively. Following ionisation due to beta irradiation, free electrons trapped at Dy^{3+} cause formation of Dy^{2+} cations whereas holes concomitantly transferred to Eu^{2+} converting these to Eu^{3+}. During heating, the electrons are released from the Dy^{2+} and recombine at the Eu^{3+} centre to produce luminescence via the 5d $\rightarrow 4f^7$ Eu^{2+} emission. Although electron transfer to the luminescence centre occur via the conduction band, this is a generic description and is not with reference to a particular excited state of the five-fold degenerate 5d energy level. Such an assignment is outside the scope of and is not essential for this discussion. We speculate that the process may also occur by quantum tunnelling. The activation energy values listed in Table 1 are consistent with ~ 1 eV associated with the Dy^{2+} supposed electron trapping state.

Regarding deep electron traps, Chernov et al., (2008) suggested that these are substitutional Dy^{3+} at different Sr host-sites. We speculate that other electron traps may include oxygen vacancies acting as F-centres or aggregates such as (Dy^{3+} + $\mathbf{O_2^{3-}}$), the latter discussed by Townsend and White (1996).

The thermoluminescence decreased with heating rate in a manner consistent with thermal quenching. The interpretation of thermal quenching in spontaneously emitted luminescence of inorganic phosphors is not identical to its meaning in thermoluminescence. In the former, thermal quenching is discussed with reference to a temperature beyond which the luminescence intensity decreases to below 50% of its value at a reference temperature (e.g. Dorenbos, 2005b). Thermal quenching in thermoluminescence is not quantified in this way but describes the significant decrease of luminescence intensity caused by the increase of measurement temperature. Thermal quenching involving Eu^{2+} in inorganic compounds, including $SrAl_2O_4$:Eu^{2+},Dy^{3+}, was discussed by Dorenbos (2005b) as due to thermal excitation of an electron in the 5d orbital to conduction band states. The electron remains bound to an Eu^{3+} ion in an exciton-pair and transits non-radiatively to the ground state of the Eu^{2+} ion.

In this work, we consider the Mott–Seitz configurational coordinate model by which radiative and non-radiative transitions to the ground state occur from two different excited state levels as relevant. Since the 5d level is degenerate, possible non-radiative and radiative are then possible.

8.2 Explanation using a model based on a continuum of energy levels

The preceding discussion was based on the assumption that electron traps form discrete single-valued localized states within the energy band gap. However, we have demonstrated that the TL from $SrAl_2O_4$:Eu^{2+},Dy^{3+} can be associated with a quasi-continuum set of electron traps. Whereas both $T_m - T_{stop}$ and $T_m - dose$ procedures imply that the main peak is a collection of first-order peaks, whole-peak methods produce general or second-order kinetics for the same peak. It is therefore necessary to reconcile these observations.

Because the thermoluminescence of $SrAl_2O_4$:Eu^{2+},Dy^{3+} suggests the presence of closely-spaced peaks, its electron trap should not be modelled as single-valued but rather as a spread of energy values about the putative electron trap. The outlines of such a model have been discussed elsewhere e.g. (Chen and McKeever, 1997). If $D(E)$ is the density of states, then the number of energy levels between E and $E + dE$ is $D(E)dE$. Therefore, the concentration of trapped electrons n is,

$$n = \int_0^{E_c} f(E)g(E)dE, \qquad (10)$$

where $f(E)$ is the probability that an energy level is occupied. The concentration of electrons in the conduction band n_c is contributed to by stimulation from traps and decreased owing to re-trapping and loss to recombination centres. Thus

$$\frac{dn_c}{dt} = \int_0^{\infty} pf(E)D(E)dE - n_c A_n \int_0^{\infty}\big(1 - f(E)\big)D(E)dE - n_c m A_{mn}, \qquad (11)$$

where p is thermal stimulation probability, A_n the retrapping probability, m the concentration of recombination centres and A_{mn} the recombination probability. Since charge neutrality requires that $n + n_c = m$, the thermoluminescence intensity I can be expressed as

$$I(t) = -\eta \frac{dm}{dt}, \qquad (12)$$

where η is the luminescence efficiency. For a continuous distribution of energy levels over a finite range $\Delta E = E_f - E_i$ under the assumption of first-order kinetics, relevant in this work, the thermoluminescence intensity I(T) becomes

$$\mathrm{I(T)} = \frac{n_o s}{\Delta E}\int_{E_i}^{E_f} \exp\left(-\frac{E}{kT}\right) \times \exp\left[-\frac{s}{\beta}\int_{T_o}^{T} \exp\left(-\frac{E}{kT'}\right) dT'\right] dE, \qquad (13)$$

where all symbols are as defined before.

The thermoluminescence intensity for a quasi-continuum set electron traps in $SrAl_2O_4$:Eu^{2+},Dy^{3+} requires that the form of its density of states $D(E)$ be known. It is not. Therefore, the analysis of a glow-peak for a particular dose necessary applies to the most dominant component of a composite because this is based on reducing the number of energy levels to one. In this sense, analyses of an experimental or digitally-mustered peak by curve-fitting are approximations. The accuracy for digitally-mustered peaks can be improved by increasing the resolution of the mustering in order to minimise the influence of other components.

Regarding the order of kinetics, Hornyak and Chen (1989) evaluated glow-peaks using Eq. (13) and noted that the qualitative features of the peak changed from first to second-order kinetics when the value of ΔE increased. This is consistent with our observation that when the main peak is analysed using a limited range e.g. $T_m - T_{stop}$ where data points are taken from a part of the peak, the order of kinetics found is first-order. On the other hand, when the peak is analysed as a simple single one, this subsumes multiple components and increases the range of ΔE explaining why the order of kinetics appears to increase from first to general or second-order kinetics.

9. Conclusion

The kinetic analysis of thermoluminescence from beta irradiated $SrAl_2O_4:Eu^{2+},Dy^{3+}$ has been studied. Using various experimental tests including partial heating, isothermal heating, phosphorescence and obliquely using fading, it has been demonstrated that the prominent peak, as the glow-curve, consist of closely-spaced peaks. Analysis of the peak for its order of kinetics using qualitative means such as the $T_m - T_{stop}$ method implies that it is subject to first-order kinetics. However, analysis using whole-peak methods produce orders of kinetics other than one. A model based on density of energy states, used to discuss the difference in results from qualitative and quantitative analysis, suggests that the presence of collocated peaks accounts for the inconclusive nature of its order of kinetics as deduced from experimental results. The activation energy is of the order of 1 eV, consistent with that of the Dy^{2+} cation, the presumed electron trapping state of the Dy^{3+} electron trap. The main peak is affected by thermal quenching with an activation energy of 0.520 ± 0.002 eV. Whereas the luminescence is ascribed to $5d \rightarrow 4f^7$ Eu^{2+} transitions, the thermal quenching is presumed to occur similarly but from an alternative level of the degenerate 5d energy level of the Eu^{2+} cation.

Acknowledgements

The author acknowledges with gratitude financial assistance from Rhodes University and the National Research Foundation of South Africa (Grant UID74438).

References

Bedyal, A.K., Vinay, K., Lochab, S.P., Fouran Singh, Ntwaeaborwa, O.M., Swart, H.C., 2013. Thermoluminescence response of gamma irradiated $SrAl_2O_4:Eu^{2+}/Dy^{3+}$ nanophosphor. Int. J. Mod. Phys., 22, 365-373.

Bos, A.J.J., van Duijvenvoorde, R.M., van der Kolk, E., Drozdowski, W., 2011. Thermoluminescence excitation spectroscopy: A versatile technique to study persistent luminescence phosphors. J. Lumin. 131, 1465-1471.

Cannas, C., Musinu, A., Peddis, D., Piccaluga, G., 2006. Synthesis and Characterization of $CoFe_2O_4$ Nanoparticles Dispersed in a Silica Matrix by a Sol−Gel Autocombustion Method. Chem. Mater. 18, 3835-3842.

Chen, R., Hag-Yahya, A., 1996. Interpretation of very high activation energies and frequency factors in TL as being due to competition between centres. Radiat. Prot. Dosim. 65, 17-20.

Chen, R., McKeever, S.W.S.,1997. Theory of Thermoluminescence and Related Phenomena. World Scientific, Singapore.

Chernov, V., Mélendrez, R., Pedroza-Montero, M., Yen., W.M., Barboza-Flores, M., 2008. The behaviour of thermally and optically stimulated luminescence of $SrAl_2O_4:Eu^{2+},Dy^{3+}$ long persistent phosphor after blue light illumination. Radiat. Meas. 43, 241-244.

Chithambo, M.L., 2014. A method for kinetic analysis and study of thermal quenching in thermoluminescence based on use of the area under an isothermal decay-curve. J. Lumin. 151, 235-243.

Chithambo, M.L., Nyirenda, A.N., Finch, A.A., Rawat, N.S., 2015. Time-resolved luminescence and spectral emission features of α-Al_2O_3:C. Physica. B: Condens. Matter. 473, 62-71.

Chithambo, M.L., Niyonzima, P., 2014. On isothermal heating as a method of separating closely collocated thermoluminescence peaks for kinetic analysis. J. Lumin. 155, 70-78.

Dorenbos, P., 2005a. Mechanism of Persistent Luminescence in Eu^{2+} and Dy^{3+} codoped aluminate and silicate compounds. J. Electrochem. Soc. 152, H107-H110.

Dorenbos, P., 2005b. Thermal quenching of Eu^{2+} 5d–4f luminescence in inorganic compounds. J. Phys.: Condens. Matter 17, 8103–8111.

Hornyak, W.F., Chen, R., 1989. Thermoluminescence and phosphorescence with a continuous distribution of activation energies. J. Lumin. 44, 73-81.

Kitis, G., Gomez-Ros, J.M., Tuyn, J.W.N., 1998. Thermoluminescence glow-curve deconvolution functions for first, second and general orders of kinetics. J. Phys. D: Appl. Phys. 31, 2636-2641.

Kshatri, D.S. Khare, A., Jha, P., 2013. Thermoluminescence studies of $SrAl_2O_4$: Eu^2 phosphors at different Dy concentrations. Chalcogenide Letters, 10. 121-129.

King, G. E., Finch, A.A., Robinson, R.A.J., Taylor, R.P., Mosselmans, J.F.W., 2011. The problem of dating quartz 2: Synchrotron generated X-ray excited optical luminescence (XEOL) from quartz. Radiat. Meas. 46, 1082-1089.

Luff, B.J., Townsend, P.D., 1993. High sensitivity thermoluminescence spectrometer. Meas. Sci. Technol. 4, 65 - 71.

Matsuzawa, T., Aoki, Y., Takeuchi, N., Murayama, Y., 1996. A new long phosphorescent phosphor with high brightness, $SrAl_2O_4:Eu^{2+},Dy^{3+}$. J. Electrochem. Soc., 143, 2670 – 2673.

Mokoena, P.P., Chithambo, M.L., Vinay Kumar, H.C. Swart, H.C., Ntwaeaborwa, O.M. 2015. Thermoluminescence of calcium phosphate co-doped with gadolinium and praseodymium. Radiat. Meas. 77, 26-33.

Nakamura, T., Kaiya, K., Takahashi, N., Matsuzawa, T., Rowlands, C.C., Beltran-Lopez, V., Smith, G.M., Riedi, P.C., 2000. High frequency EPR of europium(II)-doped strontium aluminate phosphors. J. Mater. Chem., 10, 2566 - 2569.

Pagonis, V., Kitis, G., Furetta, C., 2006. Numerical and Practical Exercises in Thermoluminescence. Springer, Berlin.

Swart., H.C., Terblans, J.J., Ntwaeaborwa, O.M., Coetsee, E., Mothudi, B.M., Dhlamini, M.S., 2009. Photon emission mechanisms of different phosphors. Nucl. Instrum. Meth. B. 267, 2630 - 2633.

Townsend, P.D., White, D.R., 1996. Interpretation of rare earth thermoluminescence spectra. Radiat. Prot. Dosim. 65, 83-88.

Wako, A.H. 2015. Tailoring Luminescence Properties of Rare Earth Doped Aluminate and Garnet Phosphors. Unpublished PhD thesis.

Wang, Y., Cui, M., Zhao, Y., Xia, Z.G., Finch, A.A., Townsend, P.D., 2016. Competing roles of defects in $SrAl2O4:Eu^{2+},Dy^{3+}$ phosphors detected by luminescence techniques. J. Mater. Res., Vol. 31, 1403 – 1412.

Figure and table captions

Figure 1. The temperature-dependence of XEOL spectra (a) and the corresponding contour map (b).

Figure 2. A glow-curve measured at 1°C s^{-1} after irradiation to 20 Gy and in the inset, the natural thermoluminescence. The background is shown for comparison.

Figure 3. T_m against T_{stop} for measurements corresponding to 20, 60 and 100 Gy. Each data point is an average of five (a) Similar measurements corresponding to 20, 60 and 100 Gy (inset) between 20 and 30°C made at 1°C intervals (b).

Figure 4. The dependence of T_m on dose. The dashed lines are only visual guides.

Figure 5. The growth-curve for the apparently-single peak for doses 10 - 155 Gy for measurement at 1°C s^{-1}. The inset shows glow-curves corresponding to 20, 60, 123 and 155 Gy.

Figure 6. Thermoluminescence measured at 1°C s^{-1} after nominal delays of 0, 5 and 10 s between irradiation and measurement (a) A glow-curve measured after beta-irradiation to ~18.9 Gy at 0.10 Gy s^{-1} (b) A thermoluminescence isometric plot recorded after X-ray irradiation to 18 Gy at 0.03 Gy s^{-1} (c).

Figure 7. Glow-peaks obtained after partial heating to 40, 45, 60, 80 and 145°C (a) the complete set of such peaks and, in the inset, those found following preheating to 180 and 270°C (b).

Figure 8. Some glow-curve components recovered using isothermal-heating at 80, 130, 240, 330 and 380℃ for 100 s respectively each corresponding to 100 Gy.

Figure 9. The effect of delayed stimulation on the thermoluminescence (a) Phosphorescence measured for 30000 s following irradiation to 100 Gy. The solid line through data is the best fit of Eq. (6) with $A = 4313.2850 \pm 10.0820$, $\kappa = 879.2642 \pm 2.8844$ and $\gamma = 288.8671 \pm 0.6810$. The residuals in the inset, consistent with zero, are evidence of a good fit (b) Glow-curves measured immediately after irradiation (x0.04) and after 3000 s; the inset shows a measurement following preheating to 100℃ intended to remove the main peak (c).

Figure 10. A glow-curve measured at 0.4°C s^{-1} (open circles) plotted alongside those obtained at 0.8°C s^{-1} (open squares) and 3°C s^{-1} (filled squares) intended to illustrate the change in size of the glow-curves with heating rate. The inset shows the same feature using peak intensities (in counts $^{o}C^{-1}$). Figure 10(b) shows ln $[(I_U/I_Q) - 1]$ against $1/kT_m$ used to evaluate the activation energy for thermal quenching.

Figure 11. A glow-curve measured following irradiation to 60 Gy (a). The inset is the same data on a semi-logarithmic scale. The residuals plot, consistent with zero, is evidence of a good fit. The first two components recovered by deconvolution are included. Figure 4(b) shows, as a function of dose, the activation energy and, the order of kinetics (inset).

Figure 12. The first five digitally-mustered components of the simple peak fitted with the Kitis model (a) Peaks obtained after partial heating at intervals from 40 through 85°C (b).

Figure 13. The dependence of the area Φ on measurement temperature.

Figure 14. The change of intensity against delay between irradiation and measurement noted as peak-intensity (open circles) and as the area under the peak (open squares). The inset shows the apparent peak position against delay.

Table 1. Kinetic parameters for $SrAl_2O_4:Eu^{2+},Dy^{3+}$ determined using various methods.

Figure 1

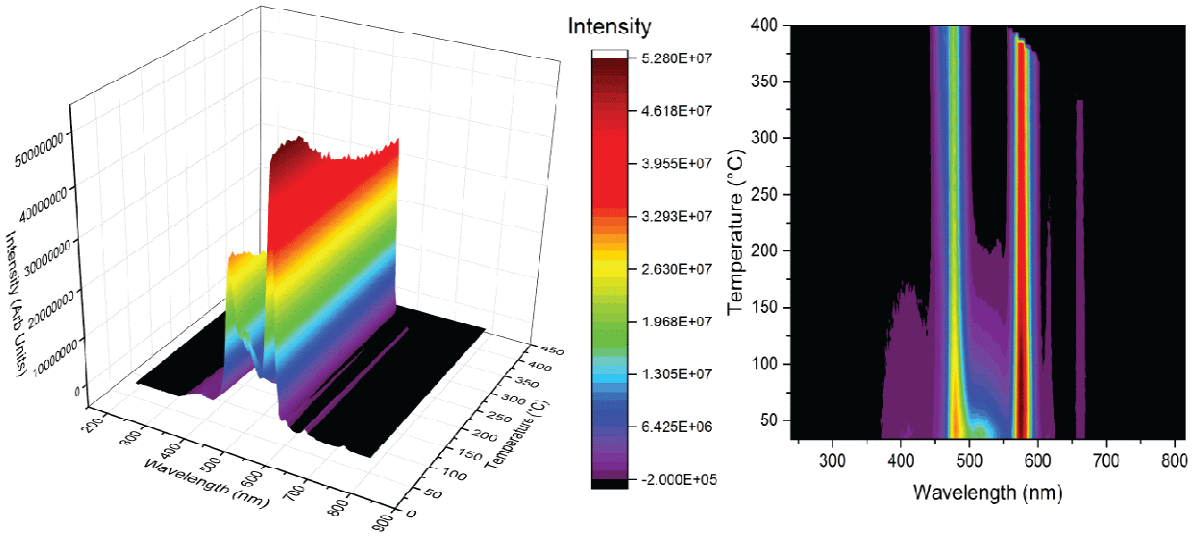

(a) (b)

Figure 2

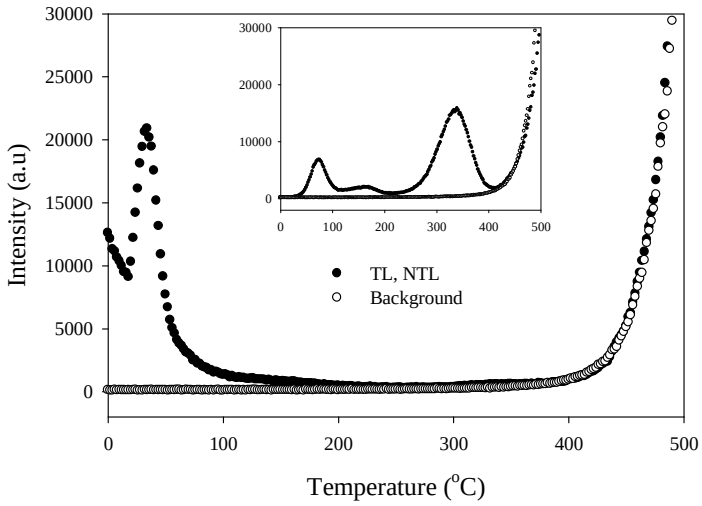

Figure 3

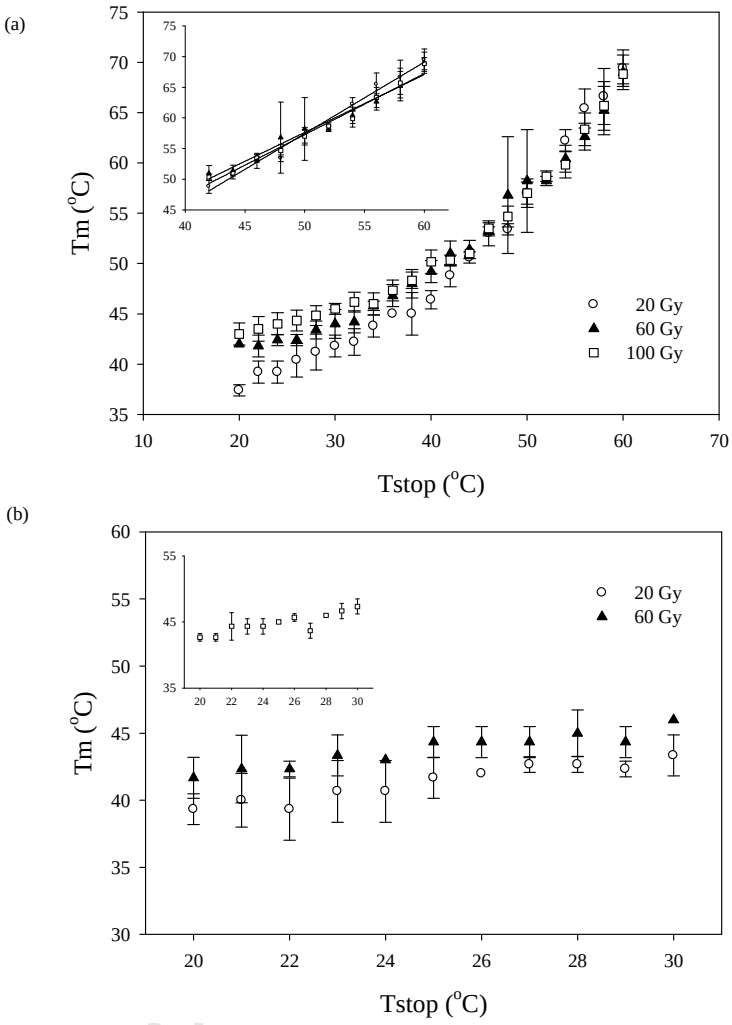

Figure 4

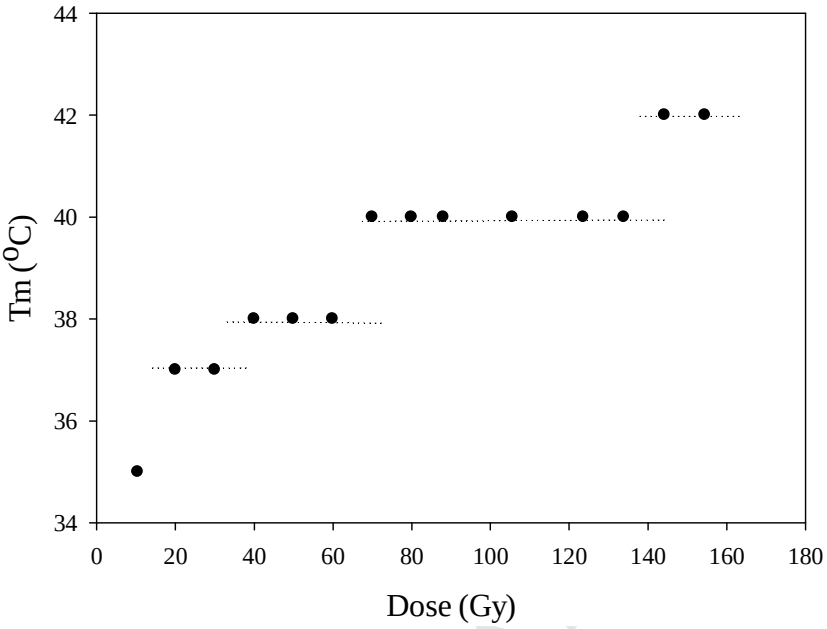

Figure 5

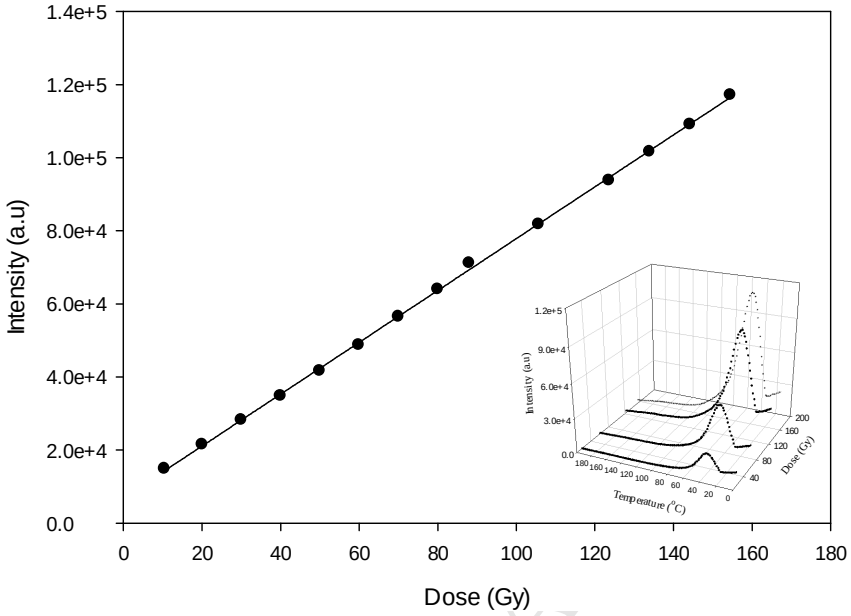

Figure 6

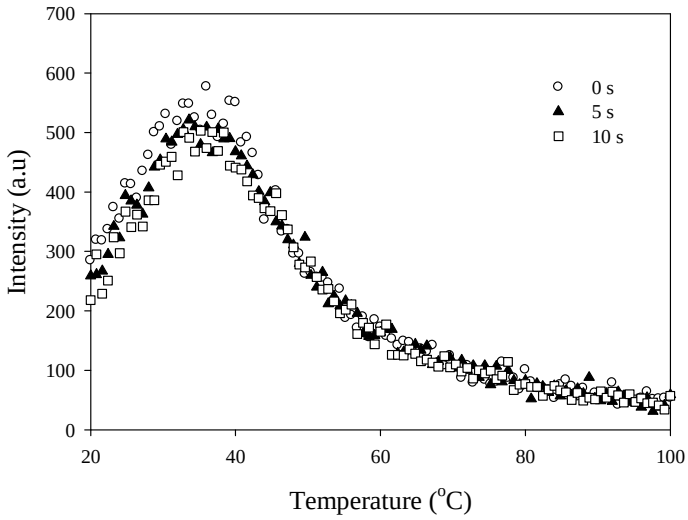
Intensity (a.u)
Temperature (°C)
0 s
5 s
10 s

(a)

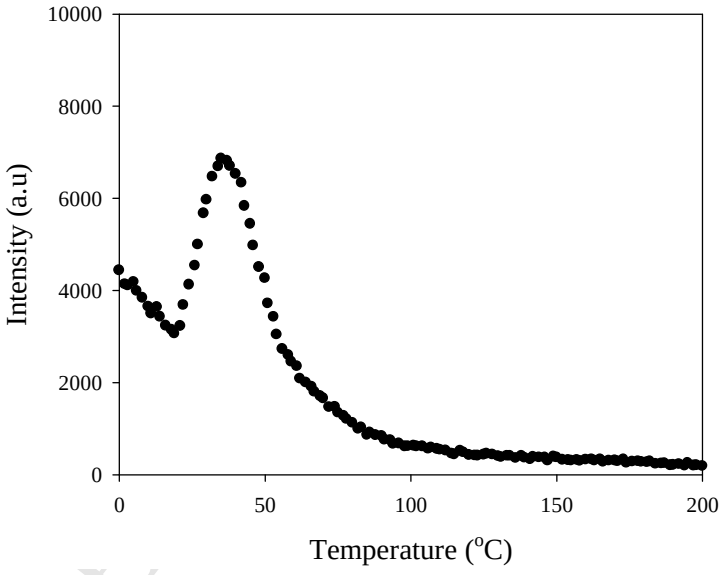
Intensity (a.u)
Temperature (°C)

(b)

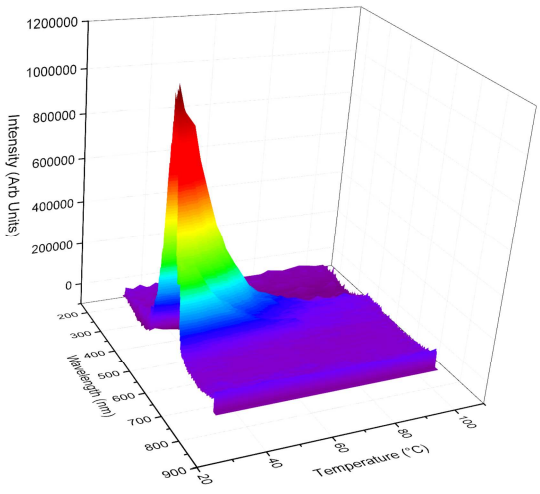
Intensity (Arb Units)
Wavelength (nm)
Temperature (°C)

(c)

Figure 7

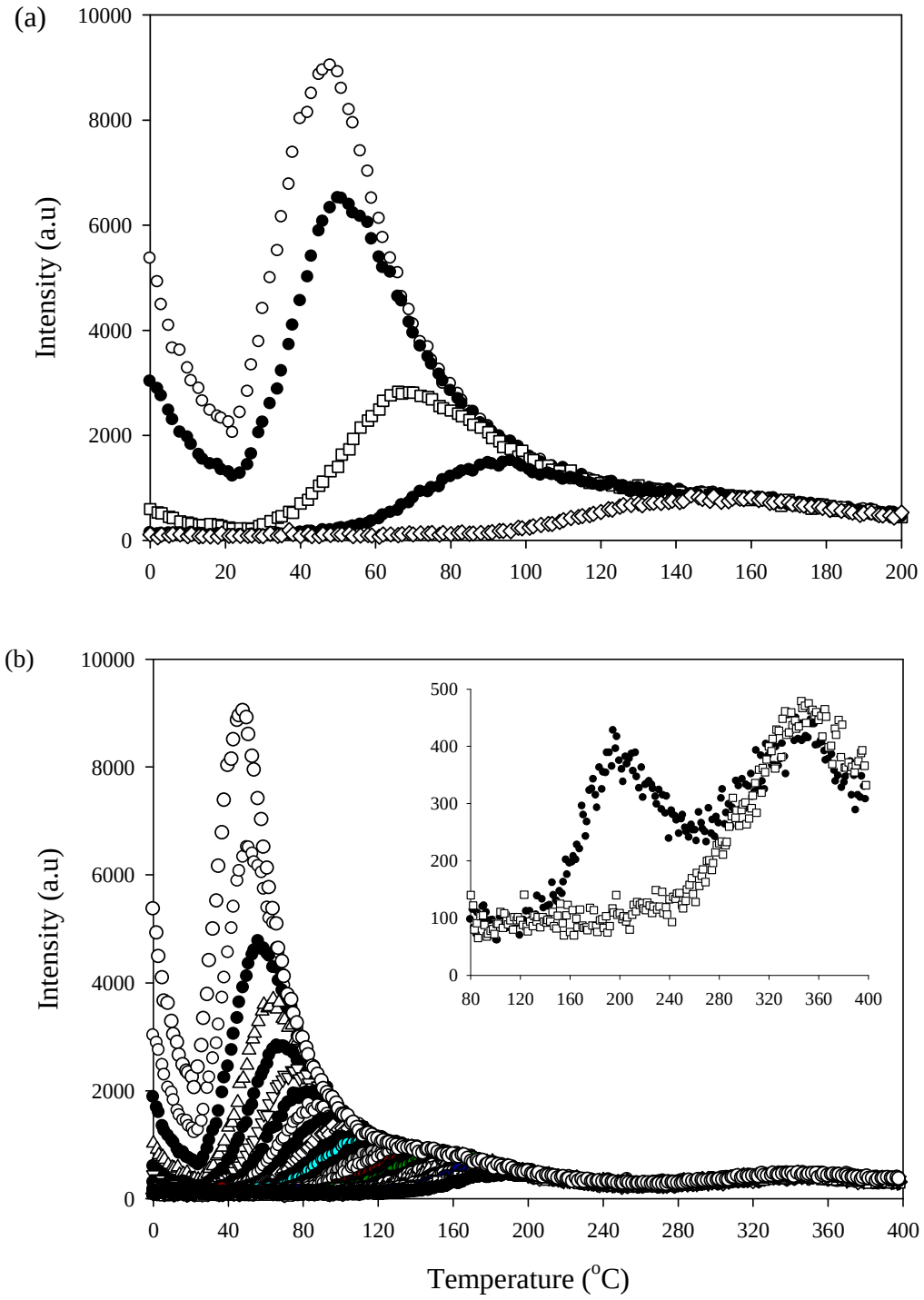
(a)
Intensity (a.u)
10000
8000
6000
4000
2000
0
0
20
40
60
80
100
120
140
160
180
200
(b)
Intensity (a.u)
10000
8000
6000
4000
2000
0
0
40
80
120
160
200
240
280
320
360
400
500
400
300
200
100
0
80
120
160
200
240
280
320
360
400
Temperature (°C)

Figure 8

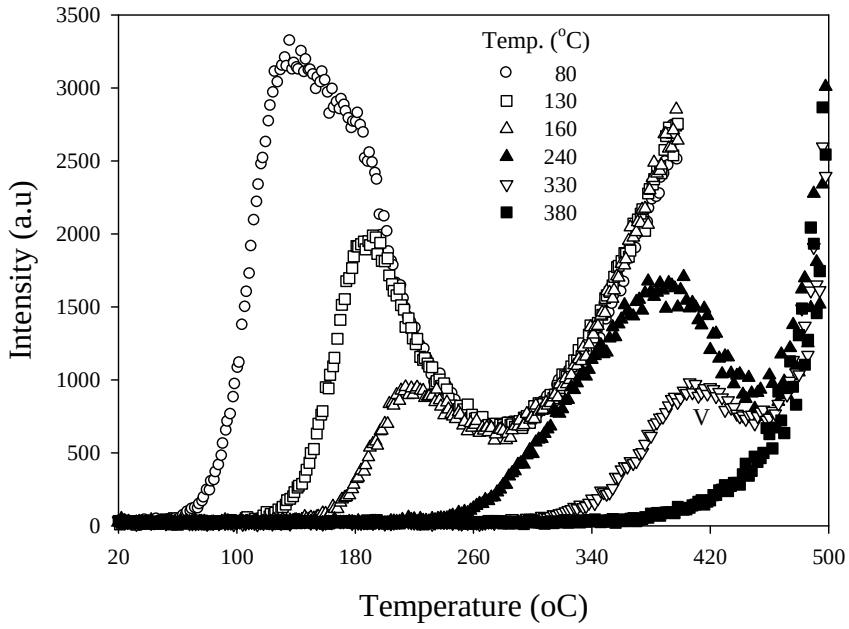

Figure 9

(a)

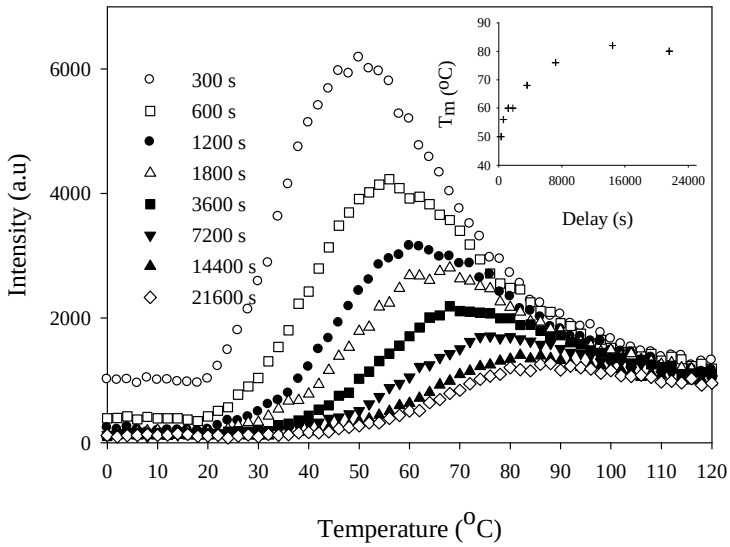
300 s
600 s
1200 s
1800 s
3600 s
7200 s
14400 s
21600 s
Intensity (a.u)
Temperature (°C)
Tm (°C)
Delay (s)

(b)

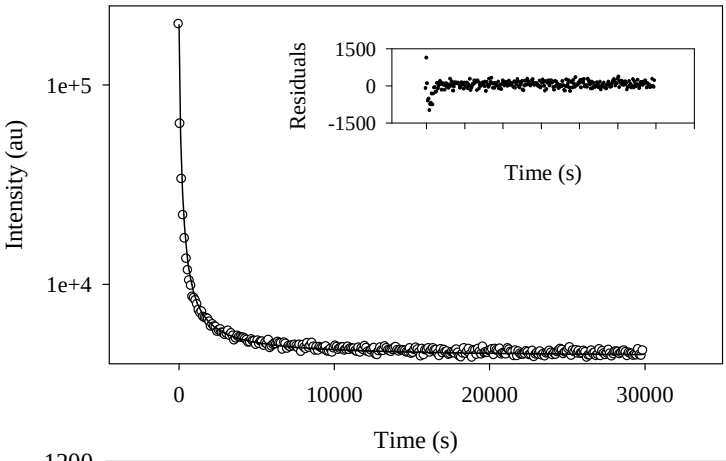
Intensity (au)
Time (s)
Residuals

(c)

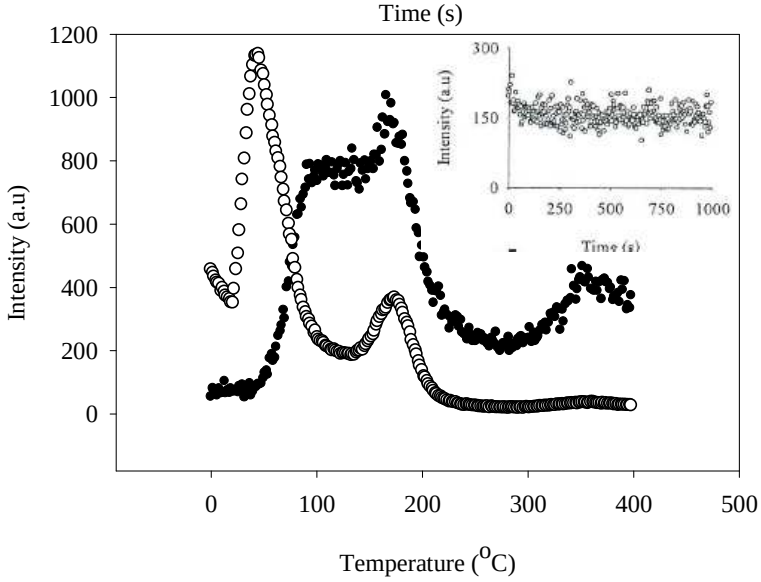
Intensity (a.u)
Temperature (°C)
Intensity (a.u)
Time (s)

Figure 10

(a)

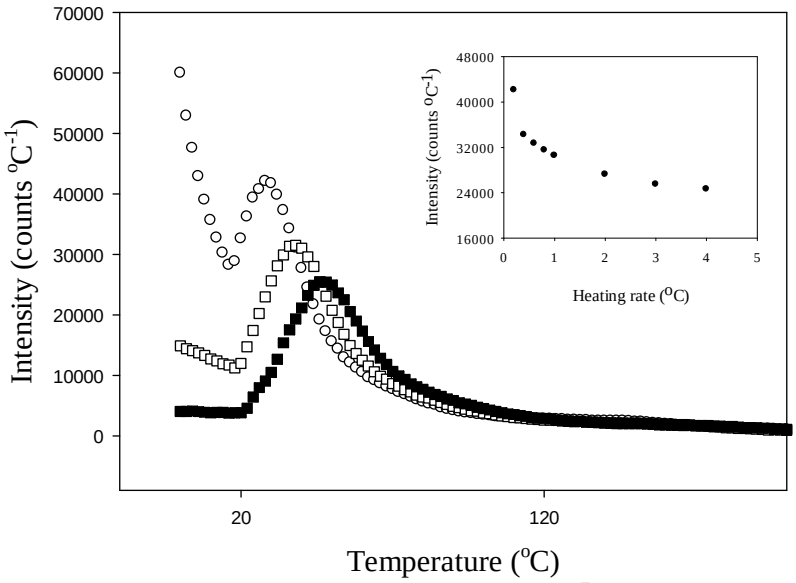
Intensity (counts °C-1)
Temperature (°C)
Intensity (counts °C-1)
Heating rate (°C)

(b)

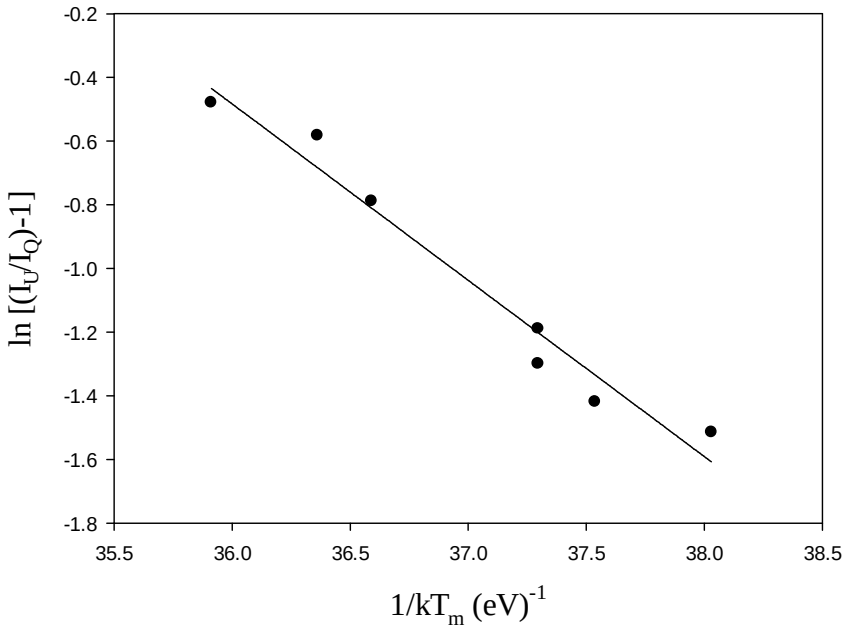
ln [(I0/IQ)-1]
1/kTm (eV)-1

Figure 11

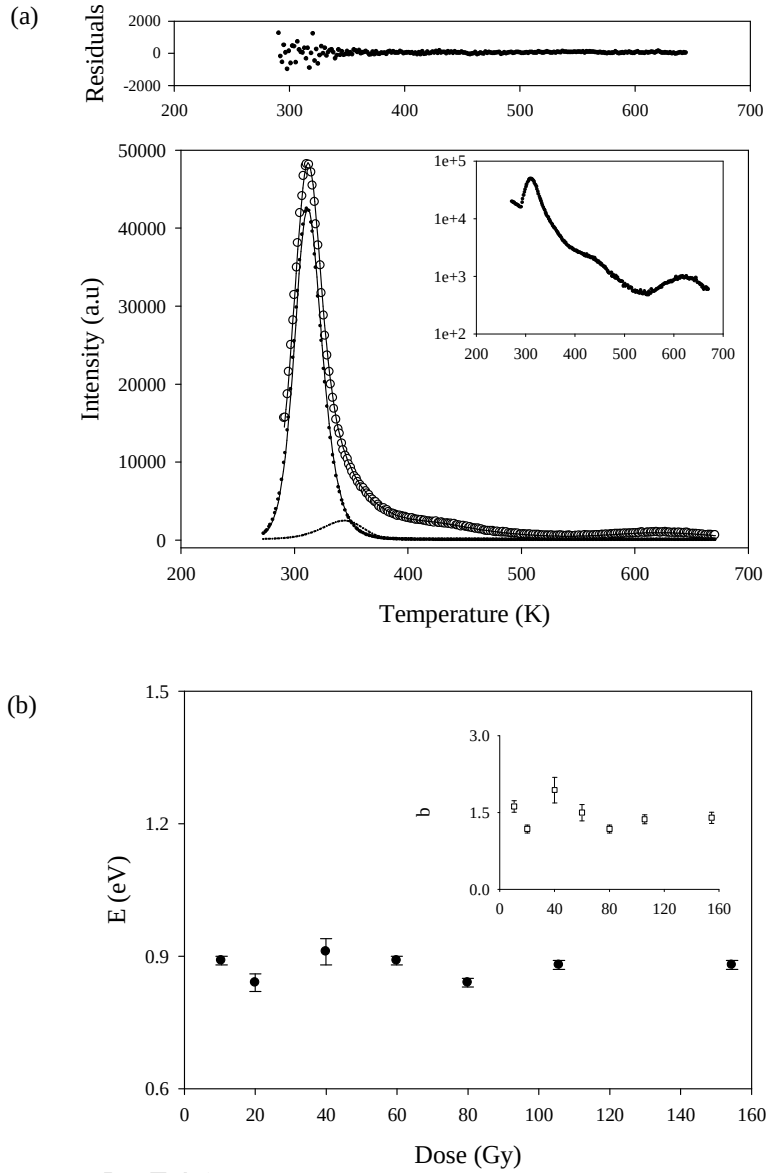
(a)
Residuals
2000
0
-2000
200
300
400
500
600
700
50000
40000
30000
20000
10000
0
Intensity (a.u)
1e+5
1e+4
1e+3
1e+2
Temperature (K)
(b)
1.5
1.2
0.9
0.6
E (eV)
3.0
1.5
0.0
b
0
40
80
120
160
0
20
40
60
80
100
120
140
160
Dose (Gy)

Figure 12

(a)

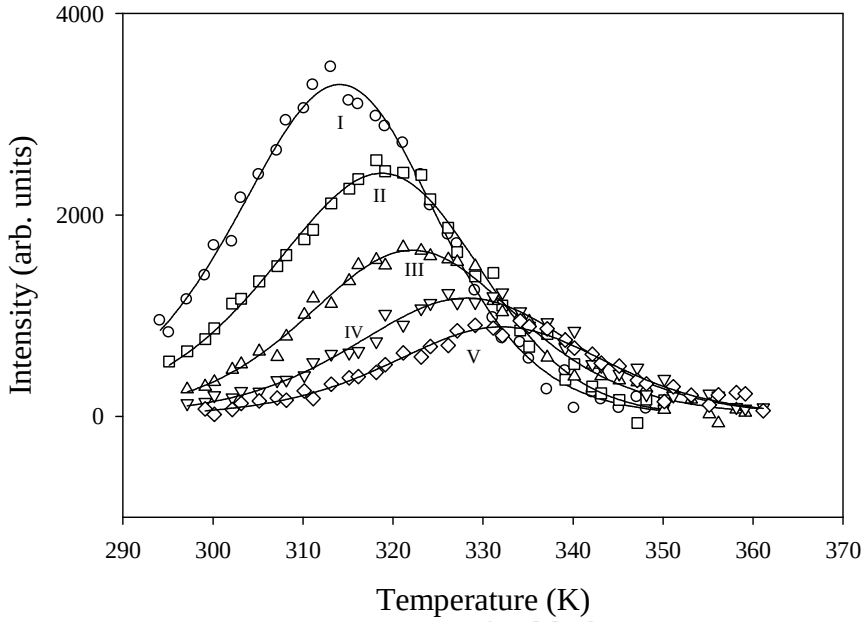
4000
2000
0
Intensity (arb. units)
I
II
III
IV
V
290
300
310
320
330
340
350
360
370
Temperature (K)

(b)

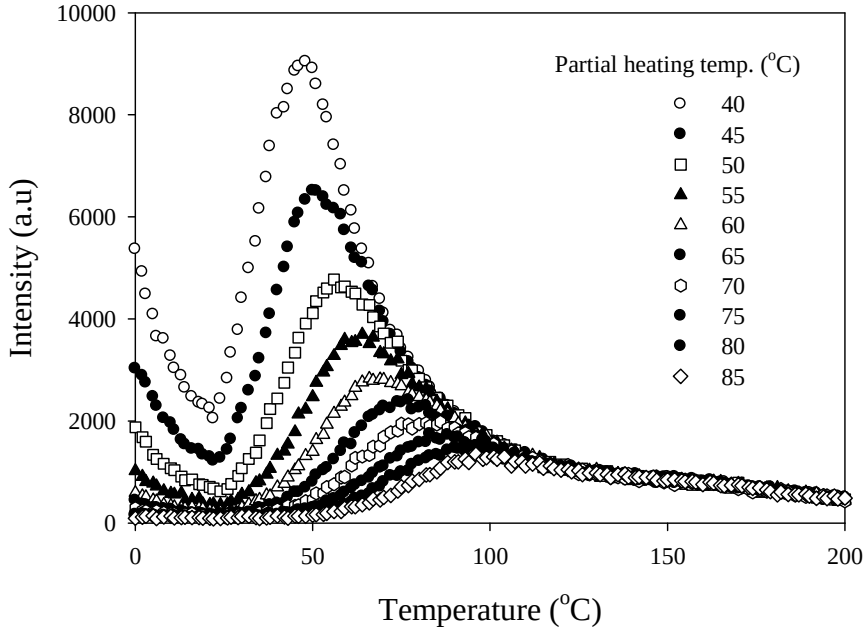
10000
8000
6000
4000
2000
0
Intensity (a.u)
Partial heating temp. (°C)
40
45
50
55
60
65
70
75
80
85
0
50
100
150
200
Temperature (°C)

Figure 13

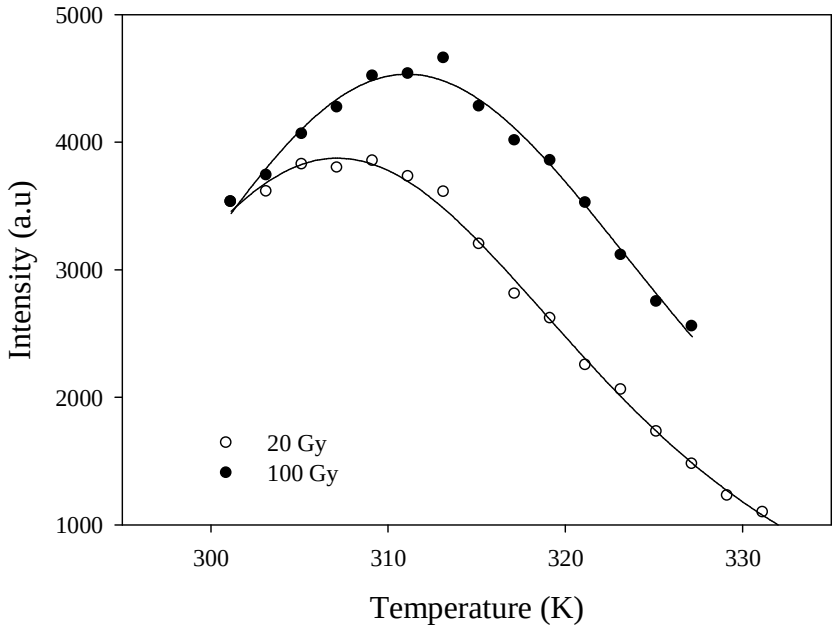

Figure 14

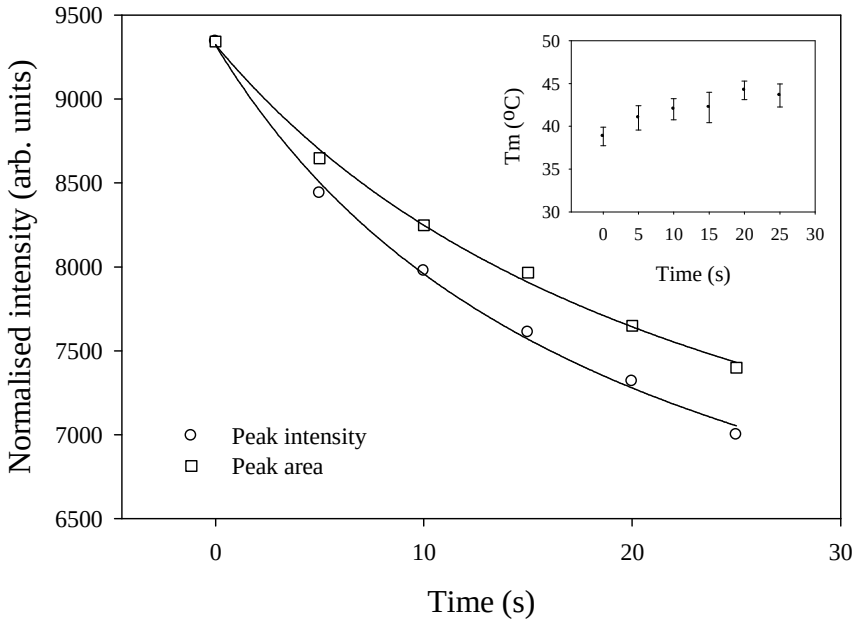

Table 1

Peak	Method	Dose (Gy	E (eV)	b	μ_g	s (s-1)	ΔE (eV)	Reference
MP	Var. heat rate	10	1.07 ± 0.06			4.1×10^{16}		Section 6.1.1
		20	1.07 ± 0.06			4.1×10^{16}		Section 6.1.1
		60	1.18 ± 0.02			1.8×10^{18}	0.54 ± 0.01	Sections 6.1.1,6.1.2
		100	1.17 ± 0.03			8.8×10^{17}	0.520 ± 0.002	Sections 6.1.1,6.1.2
	GCD	10	0.89 ± 0.01	1.62 ± 0.11		4.0×10^{13}		Section 6.2.1
		20	0.84 ± 0.02	1.18 ± 0.08		6.0×10^{12}		Section 6.2.1
		60	0.89 ± 0.01	1.51 ± 0.17		3.0×10^{13}		Fig. 11(a)
I	GCD	60	0.96 ± 0.04	1.58 ± 0.08		3.1×10^{14}		Fig. 12(a)
II		60	0.88±0.04	1.41 ± 0.09		9.0×10^{12}		Fig. 12(a)
III		60	1.02 ± 0.06	1.79 ± 0.14		1.1×10^{15}		Fig. 12(a)
IV		60	0.97 ± 0.06	1.69 ± 0.15		8.7×10^{13}		Fig. 12(a)
V		60	1.03 ± 0.07	1.69 ± 0.17		5.0×10^{14}		Fig. 12(a)
MP	Phosphorescence	20	0.87 ± 0.09	2.07 ± 0.22				Fig. 13
		100	0.84 ± 0.10	2.01 ± 0.39				Fig. 13
MP	Peak shape	20	$0.88 \pm 0.22^{\tau}$		0.50 ± 0.10			Section 6.2.4
		20	$0.87 \pm 0.21^{\delta}$		0.50 ± 0.10			Section 6.2.4
		20	$0.88 \pm 0.16^{\omega}$		0.50 ± 0.10			Section 6.2.4

- Components of a composite-peak have been illustrated and analysed
- The peak has also been analysed as it would be if it were genuinely single
- The activation energy is ~ 1 eV consistent with the theoretical value
- A model based on density of energy states has been used to augment the discussion